Flow at a separation point over a rough wall

Juliana B. R. Loureiro†
Diretoria Industrial de Metrologia Científica, Inmetro, Duque de Caxias, Rio de Janeiro

Atila P. Silva Freire†
†Programa de Engenharia Mecânica, Universidade Federal do Rio de Janeiro, C.P. 68503, 21945-970, Rio de Janeiro

Abstract. *A new data set for turbulent flow over a steep, rough hill is presented. The measurements include detailed results obtained at the separation point and in the lee of the hill. The experiments are conducted in a water channel for one particular Reynolds number. The flow conditions and the hill shape are similar to those presented in Loureiro et al. (Exp. Fluids, 42, 441-457, 2007a) for a smooth surface. As it turns out, the extent of separated flow is observed to decrease to a shorter length than that recorded by Loureiro et al. (2007a). In all, twelve measuring stations are analyzed through laser Doppler anemometry. Mean velocity as well as turbulent quantities are presented. To find the wall shear stress, global optimization algorithms are used. The merit function is defined in terms of a local solution that is shown to reduce to the classical law of the wall far away from a separation point and to the expression of Stratford at a separation point. The flow structure at the separation point is particularly discussed.*

Keywords: *Turbulence, separation, roughness*

1. Introduction

Turbulent separating flow is a research theme of utmost importance. However, the extreme difficulty on the theoretical treatment of many of its relevant issues means that much still remains to be done. The purpose of this paper is to investigate turbulent separating flows over rough surfaces. In particular, the paper discusses the structure of the turbulent boundary layer at a separation point. The solution of Stratford (1959) for the mean velocity profile, the existence of a linear shear stress region, the validity of the mixing-length hypothesis and the behaviour of the longitudinal third order moment, for example, are discussed in detail. To the present author's knowledge, this is the first time that any such theoretical discussion is accompanied by strong experimental corroboration.

Indeed, to characterize the sensitivity of separation to wall roughness, one detailed experimental study of separating flow over a rough, steep hill is presented. The measurements, as originally conducted, include detailed results obtained at the separation and reattachment points and in the reverse flow region on the lee side of the hill. This is an aspect of the experimental investigation of flow over hills that has always been known to be deficient. The flow conditions and hill shape of Loureiro et al. (2007*a*, 2007*b*) for flow over a smooth surface are here repeated for flow over a rough wall. The flow Reynolds number is increased ten fold. The separation point is observed to be pushed farther downstream, yielding a region of reverse flow shorter than that observed for flow over a smooth surface. All experiments were conducted in a water channel. Measurements were carried out through a two-beam laser Doppler velocimeter to characterize in detail the regions of attached and reversed flow.

The separation of a flow from a solid wall can be simply explained in terms of the counterplay of the convection and diffusion of vorticity within the boundary layer. In regions where the flow is strongly retarded, the convective effects remove vorticity from the boundary at a lower rate than the feeding rate of vorticity from the upstream flow. Therefore, for the velocity outside the boundary layer to decrease downstream, vorticity must be generated at the wall with the opposite sense of rotation (negative vorticity). Provided the generation of negative vorticity at the wall is sufficiently large to overcome the effects of diffusion of positive vorticity towards the wall, a reverse flow region develops over the wall. This elegant interpretation of flow separation is given by Lighthill (1986).

For turbulent flow, the rates of diffusion increase, implying that much larger adverse pressure gradients can be withstood before separation occurs. Increasing the rate of turbulent diffusion by surface roughness is a manner of delaying or even preventing separation. The qualitative role of wall roughness on flow separation has been abundantly reported in literature in connection with the so-called drag crisis. Unfortunately, no comprehensive theory – with clear and simple applicable rules – on rough wall turbulent separation has emerged.

Early experimental studies on wind tunnel flows over rough hills have sought data for locations at or upwind of the hill top but not in the wake. The main concerns were usually the characterization of flow speedup and the extent of separated flow. The motivation then was clear, linear theories (see, e.g., Jackson and Hunt 1975; Sykes 1980; Hunt et al. 1988) naturally demanded data on flow over two-dimensional low hills for model validation. Since mean velocity and turbulence measurements were conducted in wind tunnel facilities using hot- and pulsed-wire anemometers, very often only qualitative information was given on some characteristics of separated flow. Typical examples are the works of Arya et al. (1986) and of Britter et al. (1981).

More recently, the modelling emphasis has shifted to numerical schemes that consider the full non-linear time averaged

equations of motion. The impressive advances in computing power have implied that simulations previously considered unaffordable have now become routine. Turbulence models ranging from first-order eddy-viscosity through second order closure schemes have been implemented and tested against a variety of flow conditions (Castro and Apsley 1997; Ying and Canuto 1997; Hewer 1998; Ross et al. 2004). Even works on much more demanding techniques such as large-eddy simulations can nowadays be regularly found in the literature (Brown et al. 2001; Allen and Brown 2002; Iizuka and Kondo 2004).

This plethora of numerical data should naturally be accompanied by reference experimental data. Unfortunately, this is not the case if we consider the separated flow region on the lee of a hill. The existence of regions of reverse flow narrows down the choice of experimental techniques to those that can discriminate flow direction. Typical choices are then pulsed-wire anemometry (HWA), laser Doppler anemometry (LDA) and particle image velocimetry (PIV). The works of Kim et al. (1997) (HWA), of Ishihara et al. (2001) (HWA) and of Ross et al. (2004) (LDA) present wind-tunnel studies on the flow over steep hills. However, in none of these works values of the friction velocity are given.

The present work, thus, fills this important gap. Reference data are presented to comprehensively characterize the flow at a separation point. These data is then used to test the classical theories on separating flows.

2. Theoretical background

2.1 Attached and separated flows over smooth walls

For attached flows over smooth surfaces, the asymptotic diagram of the turbulent boundary layer has been shown to depend on two characteristic length scales: the thickness of the inner, viscous region ($\hat{\delta}$= ν/u_*, u_* = $\sqrt{\tau_w/\rho}$) and the thickness of the outer, defect region (δ). In fact, the classical two-layered asymptotic theories of Yajnik (1970), Mellor (1972) and Bush and Fendell (1972) are rendered true provided a small wake velocity deficit occurs. Close to a separation point, where the wake velocity is large and u_* is identical to zero, a new local scaling velocity needs to be considered. Goldstein (1948) showed this scaling velocity to be $u_{p\nu}$ (=$((\nu/\rho)\partial_x p)^{1/3}$) and the local velocity profile to assume a parabolic shape.

Under large pressure gradients, the velocity profile must be sharply curved at the wall. Since in the immediate vicinity of the wall, the inertial and turbulent terms in the Reynolds averaged Navier-Stokes equations are negligible, the viscous forces must be comparable with the pressure forces, however sharp the latter might be. Hence, the following local approximate equation applies

$$0 = -\rho^{-1}\partial_x p + \nu\partial_z^2 u. \tag{1}$$

A double integration gives Goldstein's solution

$$u = (2\nu\rho)^{-1}(\partial_x p)z^2 + (u_*^2\nu^{-1})z. \tag{2}$$

In Loureiro et al. (2007a), Eq. (2) was shown to hold over the entire flow region. In particular, it was used to find u_* and $\partial_x p$ in regions of reversed flow (see, e.g., Fig. 10). Please note that as $\partial_x p \to 0$, a linear solution is obtained.

Farther away from the wall, a new distinct region can be identified where the turbulent term gains in importance as compared to the viscous term. The existence of such region has been thoroughly discussed by Sychev and Sychev (1980), Durbin and Belcher (1992) and Cruz and Silva Freire (1998). Hence, the local approximate equation reduces to

$$\partial_z\overline{u'w'} = -\rho^{-1}\partial_x p. \tag{3}$$

A first integration gives

$$-\overline{u'w'} = (\rho^{-1}\partial_x p)z + u_*^2. \tag{4}$$

Equation (4) provides a second method to find u_* and $\partial_x p$ thorough the direct measurement of $\overline{u'w'}$. In particular, in regions where $\partial_x p \to 0$, a region of constant $\overline{u'w'}$ should be identified. At a separation point, where u_* = 0, the behaviour of $\overline{u'w'}$ in the fully turbulent region must be linear.

To further integrate Eq. (4) the turbulent term needs to be modelled. Of course, the simplest approach is to consider the eddy viscosity hypothesis together with the mixing-length model. Then, Eq. (4) can be written as

$$(\varkappa z)^2(\partial_z u)^2 = (\rho^{-1}\partial_x p)z + u_*^2, \tag{5}$$

with $\varkappa$ = 0.4 (von Karman's constant).

Two particular cases are admitted by Eq. (5). In regions where $\partial_x p \to 0$, the corresponding solution is the logarithmic law of the wall (Prandtl's solution),

$$u = \varkappa^{-1} u^* \ln z + A. \tag{6}$$

At a separation point (u_* = 0), the solution becomes (Stratford's solution (Stratford 1959))

$$u = 2\varkappa^{-1} (\rho^{-1} \partial_x p)^{1/2} z^{1/2} + B. \tag{7}$$

The above equations define a third method to determine u_* and $\partial_x p$. Plots of u against z and $z^{1/2}$ can be used to find u_* and $\partial_x p$ from the slopes of Eqs. (6) and (7) respectively, since, we have seen, $\varkappa$ = 0.4.

The general solution of Eq. (5) has been given in Cruz and Silva Freire (1998), as

$$u = 2\varkappa^{-1} \sqrt{\Delta_w} + \varkappa^{-1} u_* \ln \left((\sqrt{\Delta_w} - u_*)/(\sqrt{\Delta_w} + u_*) \right) + C, \tag{8}$$

with $\Delta_w = \rho^{-1} \tau_w + (\rho^{-1} \partial_x p) z$.

In Loureiro et al. (2007b), Eq. (8) was used as a lower boundary condition in the numerical simulation of separating flow over a steep, smooth hill. The formulation was shown to perform well in regions of attached and reversed flow. Note that under the appropriate limit processes, Eq. (8) reduces to Eqs. (6) and (7). Loureiro et al. (2007b) have also analyzed in their study the formulations of Mellor (1966) and Nakayama and Koyama (1984).

2.2 Attached and separated flow over rough walls

For flows over fully rough surfaces, the very complex flow patterns that develop around the roughness elements prevent the lower boundary condition to be specified directly on the contour of the roughness elements. The standard procedure to avoid this problem is to specify the lower boundary condition at some distance from the wall in a region where the flow statistics are spatially homogeneous.

Therefore, trivially defined parameters for flow over a smooth wall need a much deeper consideration for flow over a rough surface. The friction velocity, u_*, and the wall pressure gradient, $(\partial_x p)_w$, are not defined around the contour of the roughness elements, but, instead, at some distance from the wall where the complex flow around the individual roughness elements is not apparent anymore. Under particular conditions, provided pressure taps can be fitted around roughness elements, the method of Perry et al. (1969) can be used to find u_*. The local pressure gradient, however, has to be found from chart methods based on the local distribution of mean velocity. Note that both methods are highly inaccurate in regions of separated flow since the pressure around the roughness elements attains very low values and the existence of a logarithmic profile – a required condition for the use of chart methods – may not be granted.

The complete destruction of the viscous sub-layer by the roughness elements means that the solution of Goldstein (Eq. 2) does not hold anymore and characteristic scales dictated by the roughness itself must be brought into the problem.

For attached flows, a common practice is to re-write Eq. (6) as

$$u^+ = \varkappa^{-1} \ln((z - d)/z_0), \tag{9}$$

where z is the distance above the actual ground surface.

Thus, the specification of the lower boundary condition on rough walls is considered to depend on two characteristic scales: the roughness length, z_0, and the displacement height, d. Unfortunately, neither z_0 nor d are directly measurable quantities, but they depend on the large number of geometric parameters that are needed to characterize the roughness. In fact, depending on the way roughness elements are packed together these scales might also vary with the flow properties. Classical discussions on this problem are introduced in the papers of Perry and Joubert (1963) and Perry et al. (1969). For a recent review on the subject, readers are referred to Snyder and Castro (2002) and Castro (2007).

The solution of Cruz and Silva Freire (1998) – Eq. (8) – is valid for the fully turbulent region of the flow; as such, all details regarding the wall roughness must enter the problem through the integration parameter C. In general, in adverse pressure gradient flows, C should depend on τ_w, $\partial_x p$ and z_0. Also, any proposed functional form for C must be consistent with the logarithmic and root-squared solutions under the corresponding limits $\tau_w \gg (\partial_x p) z$ and $\tau_w \ll (\partial_x p) z$.

To recover Eq. (9) from Eq. (8) under the condition $\tau_w \gg (\partial_x p) z$, C has to be specified according to

$$C = \varkappa^{-1} u_* \left[\ln \left(4u_*^2 / ((\rho^{-1} \partial_x p) z_0) \right) - 2 \right]. \tag{10}$$

The implication is that attached and separated turbulent flows over rough surfaces can be locally represented in the fully turbulent region by

$$u = 2\varkappa^{-1}\sqrt{\Delta_w} + \varkappa^{-1}u_* \ln\left((\sqrt{\Delta_w} - u_*)/(\sqrt{\Delta_w} + u_*)\right) + \varkappa^{-1}u_* \left[\ln\left(4u_*^2/((\rho^{-1}\partial_x p)z_0)\right) - 2\right], \tag{11}$$

with $\Delta_w = \rho^{-1}\tau_w + (\rho^{-1}\partial_x p)z_T$, $z_T = z - d$.

This equation will be thoroughly tested in the following sections. However, before we do this, a few comments are in order.

We have indicated through the previous remarks how relevant wall shear stress data are for the validation of asymptotic theories. For neutral, attached flows the velocity field is known to exhibit a logarithmic solution that scales with the friction velocity, u_* (= $\sqrt{\tau_w/\rho}$). At a separation point, the velocity field follows a square-rooted behaviour, being scaled by $u_{p\nu}$ (=$((\nu/\rho)\partial_x p)^{1/3}$). This change in reference velocity has a profound influence on the asymptotic structure of the flow, and is very difficult to accommodate into a single theoretical framework (Cruz and Silva Freire 1998). Data on the local behaviour of u_* and $u_{p\nu}$ are then largely coveted by researchers for they permit the construction and validation of rational approaches to the problem.

Unfortunately, the friction velocity is a parameter very difficult to quantify. Loureiro et al. (2007*a*) have commented the various possible direct and indirect measurement techniques for flow over a smooth wall. In particular, the difficulties associated with measurements over curved surfaces were discussed. As it turns out, wall shear stress was evaluated by fitting procedures that resorted to the near wall behaviour of the velocity profile.

Graphical methods have been used abundantly on the estimation of u_*. For external boundary layers over rough surfaces this seems to be the only plausible choice together with estimations based on the shear stress profile. Of course a major drawback of these techniques is the built-in assumptions concerning the nature of the velocity and shear stress profiles – considered logarithmic and nearly uniform near the wall respectively. However, we have just seen, close to a separation point, adjustments have to be made to Eq. (9) so that coherent results are obtained. Equation (11), therefore, cannot have its importance overstated. This equation generalizes of the log- and $z^{1/2}$-laws furnishing a method to find the two unknown parameters u_* and $(\rho^{-1}\partial_x p)$ from given mean velocity profiles. Please note that in Eq. (11) z_0 and d are known parameters which must be determined independently from the undisturbed velocity field. To find u_* and $(\rho^{-1}\partial_x p)$, global optimization algorithms can then be applied on Eq. (11).

Numerical algorithms for constrained nonlinear optimization can be categorized into gradient based methods and direct search methods. Gradient-based methods use first derivatives (gradients) or second derivatives (Hessians). Direct search methods do not use derivative information and tend to converge more slowly, but can be more tolerant to the presence of noise in the function and constraints. Typically, such algorithms only build up a local model of the problems and they insist on a certain decrease of the objective function, or on a decrease of a merit function which is a combination of the objective and constraints, to ensure convergence of the iterative process. If convergent, such algorithms will only find local optima and for that reason are called local optimization algorithms.

Global optimization algorithms, on the other hand, attempt to find the global optimum, typically by allowing decrease as well as increase of the objective/merit function and consequently are computationally more expensive. Here, four direct search methods were used to determine the parameters of interest u_* and $(\rho^{-1}\partial_x p)$: Nelder Mead, Differential Evolution, Simulated Annealing and Random Search.

3. Experiments

3.1 Water channel, model hill and roughness

The experiments were carried out in the same water channel described by Loureiro et al. (2007*a*, 2007*b*). The channel is in the Hydraulics Laboratory of the Civil Engineering Department of the University of Oporto, having a total length of 17 meters. The cross section area is 0.40 m wide by 0.60 m high, and the sides and bottom of the channel are made of glass and acrylic respectively.

The water pumping system can reach a top volumetric flow rate of 150 l/s. Two pumps are used to keep the maximum flow rate variation to within $\pm$ 0.8 %. Screens and filters are used to stabilize the flow and suppress any excessive level of turbulence. They also control the size of particles in suspension. A magnetic flowmeter is used to measure the flow rate with an uncertainty of 0.001 l/s. The water level is controlled through a vertical steel gate. In this work, two flow rates were used: 2.65 and 26.76 l/s.

The hill model was placed 12 m downstream of the channel entrance. A Witch of Agnesi profile shaped the hill according to the following equation

$$z_H = H_1[1 + (x/L_H)^2]^{-1} - H_2, \tag{12}$$

where H (=$H_1 - H_2$)(= 60 mm) is the hill height and L_H (= 150 mm) is the characteristic length representing the distance from the crest to the half-height point.

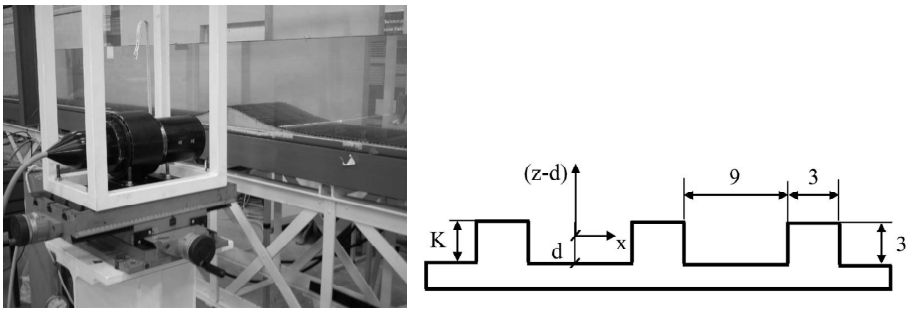

Figure 1: Illustration of model hill and details of rough surface. Dimensions are in mm. K = height of the roughness elements, d = displacement height, z = distance from the bottom of the roughness elements, z_T = z - d.

The roughness elements consisted of rigid rubber strips 3 mm wide by 3 mm high that were spaced by 9 mm . The rough surface extended from 1.5 m upstream of the hill top to 1.5 m downstream. The geometric details of the surface are given in Fig. 1; K is used to denote the height of the roughness elements, d the displacement height, z the distance from the bottom of the roughness elements and z_T = z - d.

Illustrations of the hill and of the roughness are shown in Fig. 1.

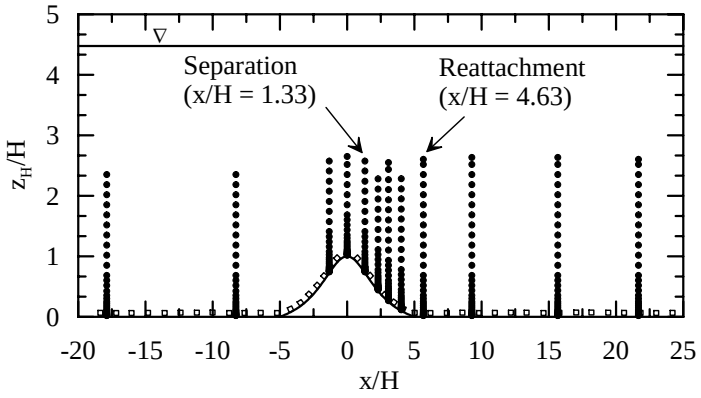

Figure 2: Location of measuring stations (conditions RSB, R_δ = 31,023). Note the origin of the coordinate system (x, z_H).

Measurements were made on the channel centerplane at the positions illustrated in Fig. 2. Regarding conditions RSB, twelve measuring stations are distributed along the flow over rough surface. The measuring positions were defined through a flow visualization study. The particular concern was to characterize well the regions of separated (τ_w = 0) and reversed flows.

3.2 Instrumentation

A two-component Dantec laser-Doppler anemometry system using an Ar-ion tube laser was operated in the forward scatter mode to measure the mean and fluctuating velocity fields. A Bragg cell unit was used to introduce an optical-electronic shift of 0.6 MHz. That was necessary to resolve the direction of the flow field and give correct measurements of near-zero mean velocities. The beams were made to pass through a series of conditioning optical elements to achieve a small measurement volume and to improve the optical alignment. A front lens with 500 mm focus length was mounted on the probe to accurately position the measurement volume on the centerline of the channel. Before being collected by the photomultipliers, the scattered light was made to pass through interference filters of 514.5 nm and 488 nm, so that only the green and blue lights were received on each photomultiplier, respectively. Table (1) lists the main characteristics of the laser-Doppler system used. The signals from the photomultipliers were band-pass filtered and processed by a burst spectrum analyzer operating in the single measurement per burst mode. A series of LDA biases were avoided by adjusting the strictest parameters on the data processor. The level validation and the signal to noise ratio were 8 and 5 respectively. For simultaneous measurements of longitudinal and vertical velocities, a coincidence window of 5000 μs was used. For the statistics at each point, 20.000 samples were considered.

Table 1: Main characteristics of the laser-Doppler system.

Wavelength	514.5nm (green) 488nm (blue)
Half-angle between beams	1.604^o
Fringe spacing	9.2μm (green) 8.7μm (blue)
Beam spacing	28mm
Beam diameter	2.2mm
Dimensions of the measurement volume	
Major axis	5.31mm (green) 5.04mm (blue)
Minor axis	149.0μm (green) 141.0μm (blue)

Typical uncertainties associated with the mean velocity data – U, W – are below 0.2% of the free stream velocity, U_δ, except in regions of reverse flow, where they increase to about 0.3%. Regarding the Reynolds stress components – $\overline{u'u'}$, $\overline{w'w'}$, $\overline{u'w'}$ – uncertainties were estimated to be 2.3%, 1.8% and 4.2% of the square of the friction velocity of the undisturbed flow, respectively, increasing to 3.8%, 3.5% and 6.9% in the reverse flow region. For the skewness and flatness factors for the longitudinal and vertical velocity fluctuations, local relative uncertainties of 3.5% and 13.9% were associated with S_u (= $\overline{u'^3}/(\overline{u'^2})^{3/2}$), S_w (= $\overline{w'^3}/(\overline{w'^2})^{3/2}$), and F_u (= $\overline{u'^4}/(\overline{u'^2})^2$), F_w (= $\overline{w'^4}/(\overline{w'^2})^2$), respectively.

4. Experimental results

4.1 General flow pattern

To place the present results into the perspective of the results of Loureiro et al. (2007*a*), we begin this section by comparing in Fig. 3 the streamlines of both experimental conditions: the smooth wall data of Loureiro et al. (2007*a*) – SS – and the new data sets RSB.

The sensitivity of flow separation to the wall roughness is apparent. In fact, the position of the separation and reattachment points can be promptly identified in Fig. 3. The exact location of these points is explicitly quoted in Table 2. The larger region of reverse flow is observed to occur over the smooth hill (Fig. 3a). For conditions RSB, the separation point is slightly displaced downstream and the region of reverse flow is reduced.

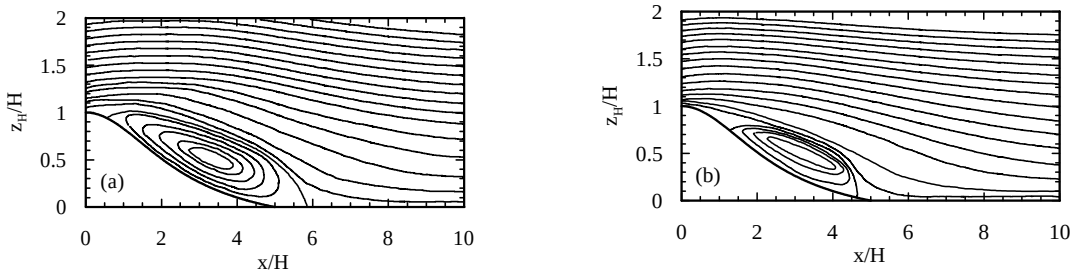

Figure 3: General pattern of reverse flow region. a: SS, b: RSB.

Table 2: Position of separation and reattachment points in x/H units.

Conditions	Separation	Reattachment	Length
SS	0.50	5.80	5.30
RSB	1.33	4.63	3.30

4.2 Undisturbed flow conditions

Loureiro et al. (2007*a*) have shown that the mean velocity profiles at stations far upstream of the hill compare to within 5% with the mean velocity profile in the absence of the hill at station x/H = 0. The same percentage was observed to

hold for the two flows over a rough surface. For this reason, the undisturbed flow properties will be here characterized in terms of the far-upstream velocity profiles.

To find u_*, d and z_0 two methods were used: the graphical method of Perry et al. (1969) and the hypothesis of Prandtl (1925) that across the wall layer the total shear stress deviates just slightly from the wall shear stress.

In the first method, the raw undisturbed velocity profiles were subtracted by a small value (e.g. 0.1 mm) from their distance to the wall. Then, a global optimization algorithm was used to find the best logarithmic fit. This process was progressively repeated – using the same subtraction step – until the curve with the best statistics could be identified.

Characteristic properties of the undisturbed profiles are listed in Table 3, together with the corresponding characteristics of the undisturbed profile of Loureiro et al. (2007*a*) for a smooth surface.

Table 3: Properties of undisturbed profile.

Property	SS	RSB
Station x/H	-12.5	-17.87
Boundary layer thickness (δ, mm)	100	100
Displacement thickness (δ_1, mm)	09	15
External velocity (U_δ, ms^{-1})	0.0482	0.3133
Friction velocity u_* (ms^{-1}) (Clauser)	0.0028	0.0204
Friction velocity u_*, (ms^{-1}) ($\overline{u'w'}$)	0.0023	0.0225
Displacement height (d, mm)	0.0	2.0
Roughness length (z_0, mm)	0.08	0.33
Longitudinal velocity fluctuations at z/δ=0.05 ($\sqrt{\overline{u'u'}}/u_*$)	2.50 1.89	
Transversal velocity fluctuations at z/δ=0.08 ($\sqrt{\overline{w'w'}}/u_*$)	0.83	1.67
Reynolds number (R_δ)	4,772	31,023
Reynolds number (R_{z_0})	0.22	6.65

To evaluate the two-dimensionality of the flow, mean velocity measurements were obtained in x-z planes located 5 cm to either side of the channel centerplane. When the hill was not in place, the results showed a variation of 2% in relation to measurements taken at the channel centerplane. In the presence of the hill, such differences in velocity measurements were of about 3%.

4.3 Longitudinal mean-velocity profiles

4.3.1 General analysis and the applicability of Eq. (11)

The applicability of Eq. (11) to attached as well as separated flows is illustrated in Figs. 4.

The overall agreement between the theoretical predictions and the experimental data was very good upstream of and at the hill top (Fig. 4). In particular, note the very well defined logarithmic region for position x/H = -17,87. These profiles correspond to the limit case $\tau_w \gg (\partial_x p)$, when Eq. (11) must reduce to Eq. (9).

4.3.2 Stratford's solution

For steady separating turbulent boundary layers, a set of definitions has been advanced in literature to characterize the different states of detachment. The following convention is normally used: ID = incipient detachment (existence of backflow 1% of time), ITD = intermittent transitory detachment (backflow 20% of time), TD = transitory detachment (backflow 50% of time), D = detachment (position where τ_w = 0). Experimental evidence suggests that TD and D are located at the same point. Therefore D, a steady parameter, is defined in terms of TD, an intermittent transitory parameter (Simpson 1996). For this reason, determining the exact wall position where flow separation occurs is not an easy task.

In the present work, the two possible profiles where the condition of detachment can be identified (τ_w = 0) are profiles x/H = 0.73 (RSA) and 1.33 (RSB). They are shown in Fig. 5 together with curve fits given by Eqs. (7) and (11). Clearly, the velocity profile at x/H = 0.73 does not follow the $z^{1/2}$-law. In fact, the negative value of u_* indicates this profile to be in the region of reverse flow. The profile at x/H = 1.33, on the other hand, is very well represented by Eqs. (7) and (11), which are almost coincident. The verification of Stratford's solution for a separating flow over a rough wall is an

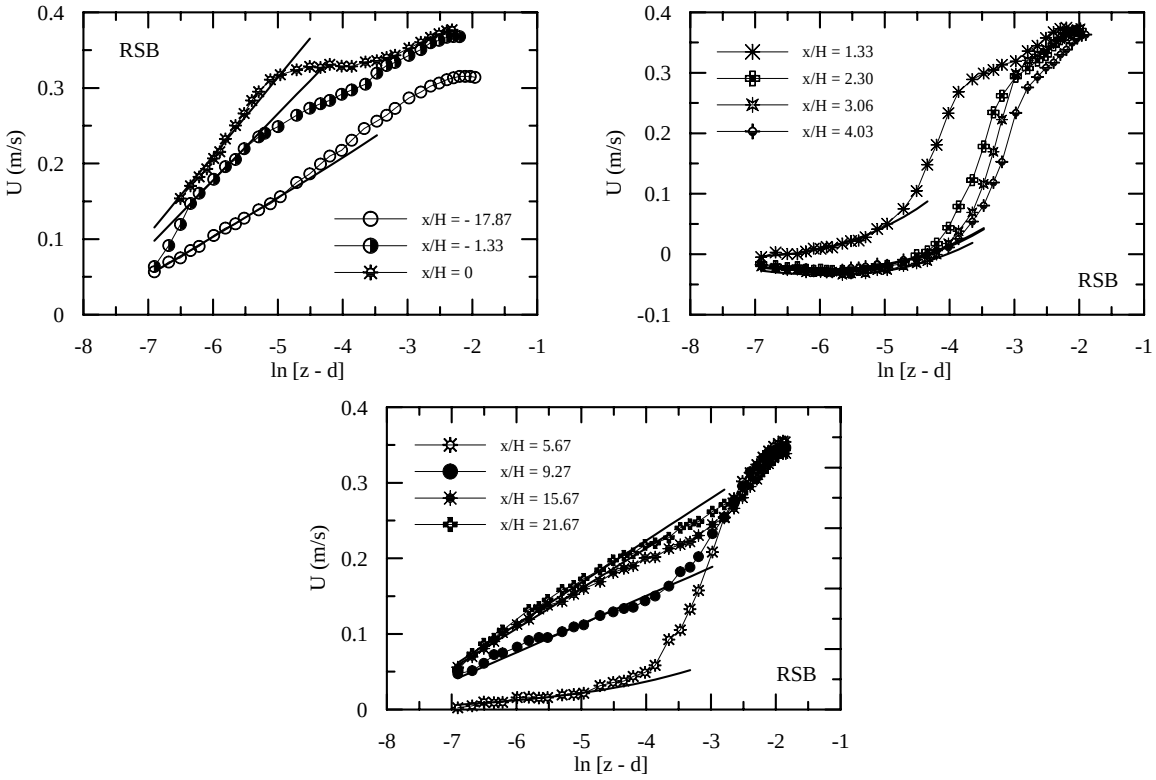

Figure 4: Mean velocity profiles upstream of and on the hill top, x-component. z = distance from the bottom of the roughness elements, d = displacement height.

important result that is rarely discussed in literature.

4.4 Second moments

4.4.1 General analysis

The changes in turbulent second moments or Reynolds stresses are of particular importance. To understand the behaviour of turbulence, Kaimal and Finnigan (1994) consider indispensable the concepts of local equilibrium, rapid distortion and turbulence memory. In particular, they discuss the reaction of the Reynolds stresses to a combination of basic strains related to flow acceleration, curvature and shear. For a complete discussion on this topic, with access to a quick guide, the reader is referred to the original source.

The changes in Reynolds stresses are shown in Fig. 6. Upstream of the hill top, in the external flow region, $\overline{u'u'}$ falls as the flow accelerates and shear decreases (Fig. 6). In the near wall region, considering the turbulence production term, $P_{uu} = -2\overline{u'w'}(\partial U/\partial z)$, the large velocity gradients (Fig. 4) give rise to $\overline{u'u'}$ peak values of about 0.035 U_δ^2 for both RSA

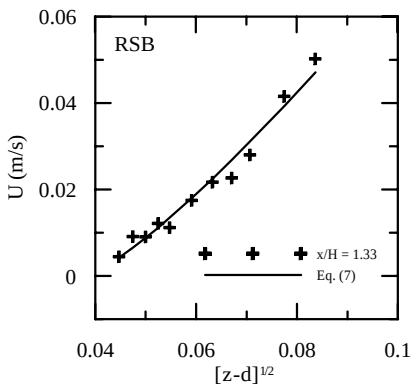

Figure 5: Stratford's solution.

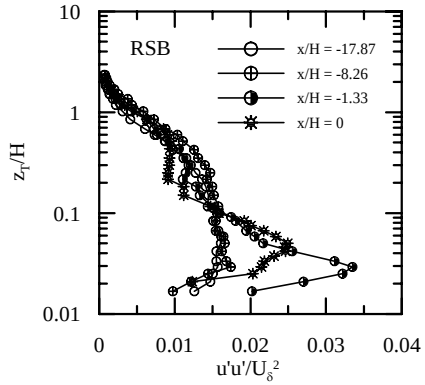

Figure 6: Normalized longitudinal Reynolds stress profiles upstream of and on the hill top. z_T = z - d, z = distance from the bottom of the roughness elements, d = displacement height.

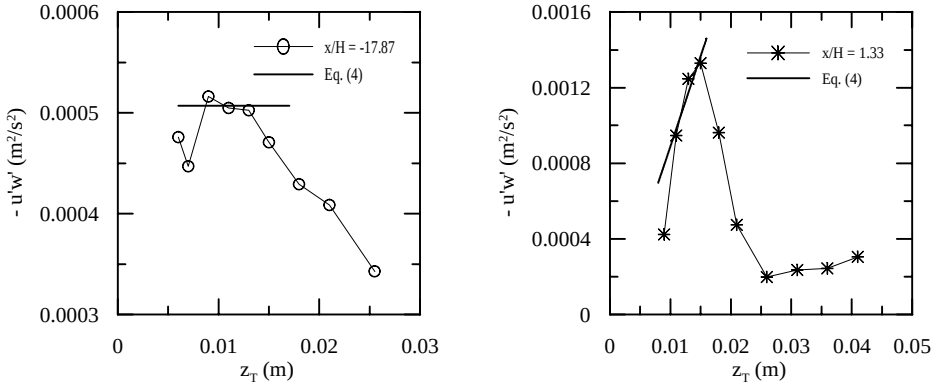

Figure 7: Shear stress profiles far away and at a separation point. z_T = z - d, z = distance from the bottom of the roughness elements, d = displacement height.

and RSB conditions. For a smooth wall, Loureiro et al. (2007*a*) recorded peak values of about 0.023 U_δ^2. On the hill top $\overline{u'u'}$ is observed to decrease in the outer region and increase in the wall region for both RSA and RSB conditions. The trends predicted by Britter et al. (1981) are then verified.

4.4.2 The applicability of Eq. (4), mixing length

Equation (4) establishes a linear relation between $\overline{u'w'}$ and $\partial_z p$. Thus, far away from regions where $\partial_z p$ is relevant, a local region where the local shear stress is constant (and approximately equal to u_*^2) should be identified. At a separation point, in particular, the profile should be linear through origin.

The $\overline{u'w'}$-profiles at stations x/H = -17.87 and 1.33 (RSB condition) are shown in Fig. 7. Note that despite the low resolution (only four to seven near wall points could be measured) regions of constant and linear shear stress can be recognized.

Since the derivation of Stratford's solution, Eq. (7), in Section 2 resorted to the mixing length concept, it might be instructive at this point to assess the validity of this hypothesis. Figure 8 shows graphs of -$\overline{u'w'}$ against $\zeta = (\varkappa z(\partial_z u))^2$ for positions x/H = -17.87 and 1.33 (RSB condition). At the separation point, the mixing length relation is observed to furnish a good representation of the local velocity behaviour provided $\varkappa$ is multiplied by 0.36. Stratford (1959) in his original work had suggested this value to be 0.66.

4.5 Third moments

Important aspects of the previous discussion can be further enlightened by consideration of the higher order moments of the fluctuating velocities. In particular, structural information can be extracted without ambiguity from third and fourth moments (Gad-el-Hak and Bandyopadhyay 1994). The triple velocity products are particularly helpful in separating flow to understand the diffusion process of the Reynolds stresses.

The skewness factor for the longitudinal velocity fluctuations is defined by

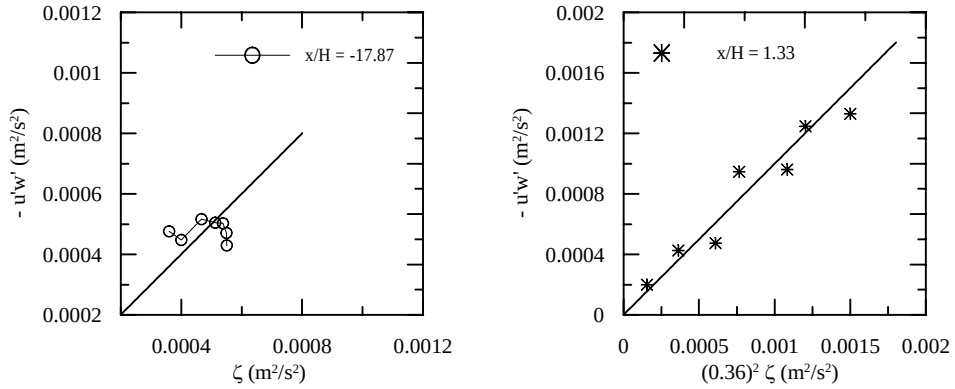

Figure 8: Mixing length profiles far away and at a separation point ($\zeta = (\varkappa z_T(\partial_{z_T}\, u))^2$).

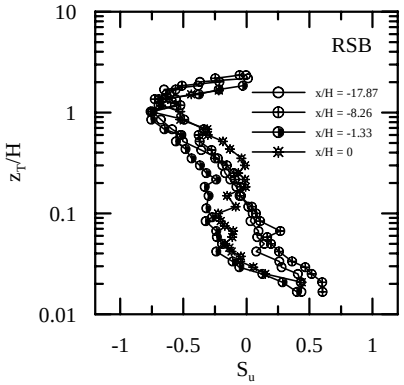

Figure 9: Skewness factor of longitudinal velocity fluctuations upstream of and on the hill top. z_T = z - d, z = distance from the bottom of the roughness elements, d = displacement height.

$$S_u = \overline{u'^3}/\left(\overline{u'^2}\right)^{3/2}, \tag{13}$$

Equivalent expressions can be written for the other flow properties. A signal with a Gaussian distribution satisfies S_u = 0.

4.5.1 General discussion

For flow over a smooth wall, S_u is positive in the near wall region and negative in the external. Flow regions where S_u is positive are associated with acceleration-dominated velocity fluctuations resulting from the arrival of external high-speed fluid (sweep events) (Gad-el-Hak and Bandyopadhyay 1994). Fernholz and Finley (1996) remark that peak values of $\overline{u'u'}$ lie in the range $13 \leq z^+(= zu_*/\nu) \leq 17$ so that the extremal values for S_u and F_u should also occur in this interval. In the log region, $20 \leq z^+ \leq 500$, S_u and F_u take on the nearly constant values 0 and 2.8 respectively. The implication is that over a large flow region the velocity fluctuations should follow nearly a Gaussian distribution. Bandyopadhyay and Watson (1988) claim that the general qualitative distributions of S and F are the same for flows over smooth and rough walls, the only significant change being the lower values of S_w (the skewness of the vertical velocity fluctuations) for all rough surfaces.

The present data show that upstream of and at the hill top, S_u follows the canonical behaviour (Fig. 9). Intense fluctuations are recorded positive near to the wall (≈ 0.5) and negative in the external region (≈ -0.75). It is also apparent that the point of cross-over from positive to negative S_u moves inward as the hill top is approached.

4.5.2 Third order closure model

Several transport models for the third moments have been presented in literature. One of the simplest propositions is that of Daly and Harlow (1970), who postulate

$$\overline{u_i u_j u_k} = \Gamma\, \tau\, \overline{u_k u_l} \partial_l(\overline{u_i u_j}) \tag{14}$$

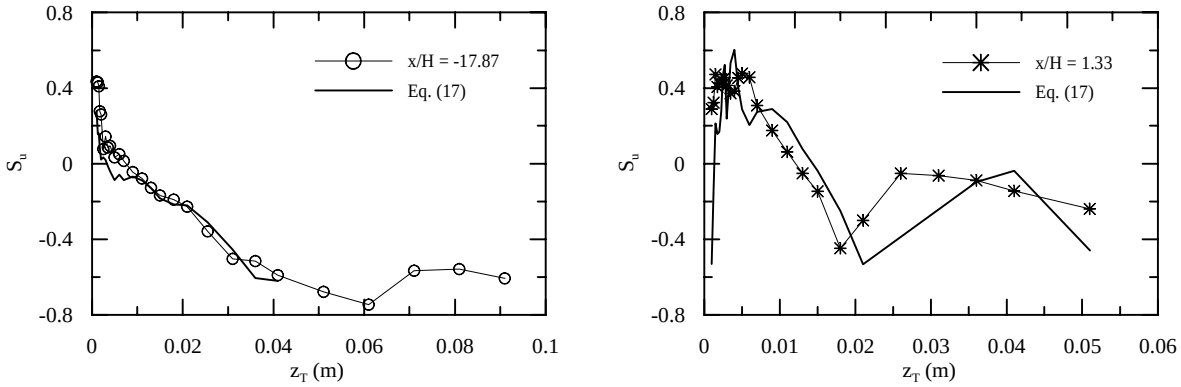

Figure 10: Profiles for the longitudinal third moments far away and at a separation point. z_T = z - d, z = distance from the bottom of the roughness elements, d = displacement height.

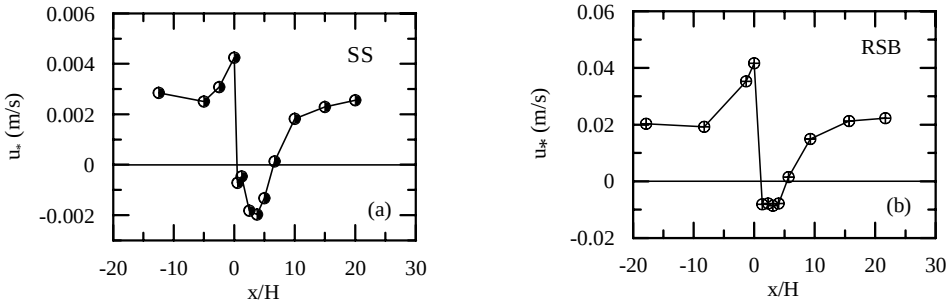

Figure 11: The behaviour of u_* for all three flow conditions.

with τ = κ/ϵ, and Γ = -0.25.

This expression has been tested in Fig. 10 for the longitudinal third moments. Two positions are considered: x/H = -17.87 and 1.33 (RSB condition). Please note the very distinct behaviour of S_u far away and near to a separation point. We had previously mentioned that at x/H = -17.87 S_u reaches a very high value near the wall, dips continuously to a negative peak value and recovers to zero. At the separation position, S_u is observed to vary much more violently. Starting from zero at the wall, S_u increases to a maximum value, dips sharply to a negative peak value and recovers quickly again to about zero. Despite the differences, Eq. (14) is observed to match very well the experiments. The near behaviour of S_u is particularly well represented at x/H = 1.33.

For flow over a rough surface, the multiplying constant Γ was found to be 1.1.

4.6 Skin-friction results

The usefulness of Eq. (11) to find the wall shear stress is illustrated next.

Predictions of u_* are shown in Fig. 11 for both rough surface conditions. Results concerning the smooth-wall flow, condition SS, have also been included for the sake of theory validation.

The agreement between results provided by Eq. (11) and the smooth wall data of Loureiro et al. (2007*a*) is accurate to within 3% even in the region of separated flow. Through the previously described optimization process, Eq. (11) can capture all the relevant friction velocity features. The region of rise before the hill top, the position of the separation point, the length of the separated flow region, the return to equilibrium condition, these are features that are all well predicted by the present procedure.

The influence of wall roughness is also well modelled. The increase in the undisturbed values of u_* for conditions RSB as a function of the roughness and of the external flow Reynolds number are in accordance with estimation methods based on the classical law of the wall. The extent of separated flow is also very well predicted when compared with Fig. 3.

Table 4 shows the results for the separation point x/H = 1.33. Note that by definition Eq. (7) implies u_* = 0. The fitting procedure yields B = -0.047103. The agreement between results given by Eqs. (4) and (9) is very good. The discrepancy exhibited by Eq. (7) results from the value of $\varkappa$ used, the canonical value 0.4.

Table 4: Skin-friction velocity predictions at the separation point x/H = 1.33.

Eq.	u_* (ms^{-1})	$\rho^{-1}\partial_x p$ (ms^{-2})
(4)	-0.0082626	0.095585
(7)	0.0	0.049461
(9)	-0.008088	0.088580

5. Final remarks

The present work is a necessary complement to the work of Loureiro et al. (2007*a*). In that work, flow over a steep, smooth hill was studied with the purpose of providing reference data for the validation of asymptotic theories and numerical simulations. Thus, a particular emphasis was placed in the accurate determination of the wall shear stress, which was evaluated from polynomial fits to the near wall mean-velocity data.

Here, two extra flow conditions were experimentally studied. These conditions contemplated flow over a rough surface and the same hill geometry but different external flow conditions. Considering the thirteen measurement stations of Loureiro et al. (2007*a*, 2007*b*), the complete set of data encompasses 36 stations. This body of data provides a rigorous account of flows with separation, furnishing reference data that can be used confidently to validate proposed models for separated flow.

Results on two-component mean flow quantities and higher-order statistical quantities were presented. Data for the shear and normal components of the Reynolds stress tensor and the distributions of skewness and flatness factors for the streamwise and vertical velocity fluctuations were thoroughly investigated.

Such a comprehensive experimental characterization of the flow field is rarely seen in literature. In special, an analysis of the near wall region based on local solutions of the motion equations was carried out, which resulted in local predictions for the wall shear stress including the regions of reverse flow. No other such work could be identified in literature with the same content.

6. Acknowledgements

JBRL benefited from a Research Fellowship from the Brazilian Ministry of Science and Technology through Programme Prometro (Grant No 554391/2006-6). ASM benefited from a Research Scholarship from the Brazilian National Research Council (CNPq). ASM is also thankful to the Rio de Janeiro Research Foundation (FAPERJ) (Grant No E-26/171.198/2003) for the concession of further financial help regarding his stay at Oporto University. APSF is grateful to the Brazilian National Research Council (CNPq) for the award of a Research Fellowship (Grant No 306977/
2006-0). The work was financially supported by CNPq through Grants No 477392/2006-7 and No 476091-2007/1, and by the Rio de Janeiro Research Foundation (FAPERJ) through Grants E-26/171.346/2005 and E-26/171.198/2003. ASM, JBRL and FTP are grateful to Prof. Maria Fernanda Proença of the Hydraulics Laboratory of Oporto University for all her help in setting up the flow rig, as well as for some very interesting technical discussions.

Allen B, Brown AR (2002) Large-eddy simulation of turbulent separated flow over rough hills. Bound Layer Meteorol 102:177–198

Arya SPS, Gadiyaram PS (1986) An experimental study of flow and dispersion in the wakes of three-dimensional low hills. Atmos Environ 20:729–740

Bandyopadhyay PR, Watson RD (1988) Structure of rough-wall turbulent boundary layer. Phys Fluids 31:1877–1883

Britter RE, Hunt JCR, Richards KJ (1981) Air flow over a two-dimensional hill: studies of velocity speedup, roughness effects and turbulence. Q J R Meteorol Soc 107:91–110

Brown AR, Hobson JM, Wood N (2001) Large-eddy simulation of neutral turbulent flow over rough sinusoidal ridges. Bound Layer Meteorol 98:411–441

Bush WB, Fendell FE (1972) Asymptotic analysis of turbulent channel flow and boundary layer flow. J Fluid Mech 56:657–681

Castro IP, Apsley DD (1997) Flow and dispersion over topography: a comparison between numerical and laboratory data for two-dimensional flows. Atmos Environ 31:839–850

Castro IP (2007) Rough-wall boundary layers: mean flow universality. J Fluid Mech 585:469–485

Cruz DOA, Silva Freire AP (1998) On single limits and the asymptotic behaviour of separating turbulent boundary layers. Int J Heat Mass Transfer 41:2097–2111

Daly JR, Harlow IH (1970) Transport equations in turbulence, Phys Fluids 13: 2634–2649

Durbin PA, Belcher SE (1992) Scaling of adverse-pressure-gradient turbulent boundary layers. J Fluid Mech 238: 699–

722
Fernholz HH, Finley PJ (1996) The incompressible zero-pressure-gradient turbulent boundary layer: an assessment of the data. Prog Aero Sci 32:245-311
Gad-el-Hak M, Bandyopadhyay PR (1994) Reynolds number effects in wall-bounded turbulent flows. Appl Mech Review 47:307–365
Goldstein S (1948) On laminar boundary layer flow near a position of separation. Q J Mech Appl Maths 1:43–69
Hewer BJ (1998) Non-linear numerical model predictions of flow over an isolated hill of moderate slope. Bound Layer Meteorol 87:381–408
Hunt JCR, Leibovich S, Richards KJ (1988) Turbulent shear flow over low hills. Quart J Roy Meteorol Soc 114:1435–1470
Iizuka S, Kondo H (2004) Performance of various sub-grid scale models in large-eddy simulations of turbulent flow over complex terrain. Atmos Environ 38:7083-7091
Ishihara T, Fujino Y, Hibi K (2001) Wind tunnel study of separated flow over a two-dimensional ridge and a circular hill. J Wind Eng 89:573-576
Jackson PS, Hunt JCR (1975) Turbulent wind flow over a low hill. Q J R Meteorol Soc 101:929–955
Kaimal JC, Finnigan JJ (1994) Atmospheric Boundary Layer Flows, Oxford University Press
Kim HG, Lee CM, Lim HC, Kyong NH (1997) An experimental and numerical study on the flow over two-dimensional hills. J Wind Engng Ind Aero 66:17–33
Lighthill J (1986) An informal introduction to theoretical fluid mechanics, C.U.P.
Loureiro JBR, Pinho FT, Silva Freire AP (2007*a*) Near wall characterization of the flow over a two-dimensional steep smooth hill. Exp Fluids 42:441–457
Loureiro JBR, Soares DV, Fontoura Rodrigues JLA, Pinho FT, Silva Freire AP (2007*b*) Water tank and numerical model studies of flow over steep smooth two-dimensional hills. Bound Layer Meteorol 122:343–365
Mellor GL (1966) The effects of pressure gradients on turbulent flow near a smooth wall. J Fluid Mech 24:255–274
Mellor GL (1972) The large Reynolds number, asymptotic theory of turbulent boundary layers. Int J Engng Sci 10:851–873
Nakayama A, Koyama H (1984) A wall law for turbulent boundary layers in adverse pressure gradients. AIAA J 22:1386–1389
Perry AE, Joubert PN (1963) Rough-wall boundary layers in adverse pressure gradients. J Fluid Mech 17:193–211
Perry AE, Schofield WH, Joubert PN (1969) Rough-wall turbulent boundary layers. J Fluid Mech 37:383–413
Prandtl L (1925) Über die ausgebildete Turbulenz. ZAMM 5:136–139
Ross AN, Arnold S, Vosper SB, Mobbs SD, Nixon N, Robins AG (2004) A comparison of wind-tunnel experiments and numerical simulations of neutral and stratified flow over a hill. Bound Layer Meteorol 113:427–459
Simpson RL (1996) Aspects of turbulent boundary-layer separation. Prog Aero Sci 32:457-521
Snyder WH, Castro IP (2002) The critical Reynolds number for rough-wall boundary layers. J Wind Eng Ind Aerodyn 90:41–54
Stratford BS (1959) The prediction of separation of the turbulent boundary layer. J Fluid Mech 5:1–16
Sychev VV, Sychev Vik V (1980) On turbulent separation. USSR Comput Maths Math Phys 20:133–145
Sykes RI (1980) An asymptotic theory of incompressible turbulent boundary-layer flow over a small hump. J Fluid Mech 101:647–670
Ying R, Canuto VM (1997) Numerical simulation of the flow over two-dimensional hills using a second-order turbulence closure model. Bound Layer Meteorol 85:447-474
Yajnik KS (1970) Asymptotic theory of turbulent shear flow. J Fluid Mech 42:411–427